In Vitro Effect of Cryptophycin 52 on Microtubule Assembly and Tubulin: Molecular Modeling of the Mechanism of Action of a New Antimitotic Drug†

P. Barbier,‡ C. Gregoire,‡ F. Devred,‡ M. Sarrazin,§ and V. Peyrot*,‡

UMR-CNRS 6032, Faculté de Pharmacie, and Laboratoire de Biophysique 1, Faculté de Pharmacie, 27 Boulevard Jean Moulin, 13385 Marseille Cedex 5, France

Received May 7, 2001; Revised Manuscript Received July 20, 2001

ABSTRACT: Cryptophycin 52 (C52) is a new synthetic compound of the cryptophycin family of antitumor agents that is currently undergoing clinical evaluation for cancer chemotherapy. The cryptophycin class of compounds acts on microtubules. This report details the mechanism by which C52 substoichiometrically inhibits tubulin self-assembly into microtubules. The inhibition data were analyzed through a model described by Perez-Ramirez [Perez-Ramirez, B., Andreu, J. M., Gorbunoff, M. J., and Timasheff, S. N. (1996) *Biochemistry 35*, 3277−3285]. We thereby determined the values of the apparent binding constant of the tubulin−C52 complex to the end of a growing microtubule (K_i) and the apparent binding constant of C52 to tubulin (K_b). The binding of C52 depended on tubulin concentration, and binding induced changes in the sedimentation pattern of tubulin, which indicates that C52 induces the self-association of tubulin and tubulin aggregates other than microtubules. Using analytical ultracentrifugation and electron microscopy, we show that C52 induces tubulin to form ring-shaped oligomers (single rings). We also show that C52 inhibits the formation of double rings from either GTP− or GDP−tubulin. In addition, the advances made by electron crystallography in understanding the structure of the tubulin and the microtubule allowed us to visualize the putative binding site of C52 and to reconstruct C52-induced ring oligomers by molecular modeling.

The microtubule network is an essential component of the cytoskeleton of eukaryotic cells. The discovery of the binding of the cytostatic drug colchicine to tubulin was a fundamental step in the development of antimitotic drugs. The development of new antimitotic drugs then led to new cancer chemotherapy approaches and to a better knowledge of microtubule pharmacology and biochemistry. Most cancer drugs have been isolated from plants: the taxoids paclitaxel and docetaxel and the vinca alkaloids vinblastine and vincristine. Paclitaxel induces microtubule polymerization and favors the lateral association of tubulin molecules in the microtubule wall (*1*). The vinca alkaloids inhibit microtubule polymerization and induce tubulin self-association into linear polymers, which lead to the formation of paracrystals in vitro from pure tubulin (*2*) and in vivo (*3*). Many compounds have been discovered that inhibit cell proliferation with an apparent action on microtubules (*4*). Many of these compounds have shown promise as potential chemotherapeutic agents in tumor models. Among these are the cryptophycins, cytotoxic depsipeptides isolated from cyanobacteria of the genus *Nostoc* (*5*). The parent molecule, cryptophycin 1, inhibits cell proliferation by blocking cell cycle progression at the prometaphase/metaphase of mitosis at picomolar concentrations with an action on microtubules. In vitro, cryptophycin 1 binds tightly to tubulin, inhibits microtubule assembly (*6*), and suppresses microtubule dynamic instability (*7*). Cryptophycin 1 competitively inhibits dolastatin 10 binding to tubulin and noncompetitively inhibits the binding of vinblastine to tubulin. Cryptophycin 1 induces the formation of small ring-shaped oligomers of tubulin (*8*). These structured oligomers resemble the tubulin aggregates induced by vinblastine. Cryptophycin 52 (C52),[1] a new synthetic member of the cryptophycin family (*9*), is currently undergoing clinical evaluation for cancer chemotherapy (Chart 1). In 1998, Panda et al. (*10*) reported that the binding of a few C52 molecules to the plus end of microtubules induces the suppression of microtubule dynamics. Panda et

Chart 1

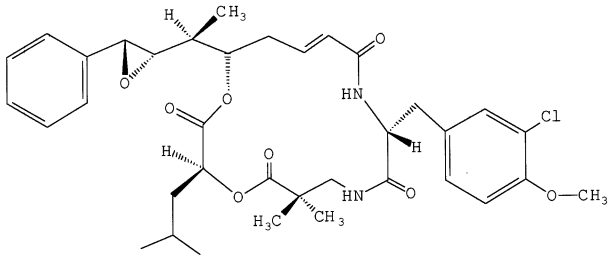

† This research was supported by grants from la Ligue Contre le Cancer (1999−2000, 2000−2001) and Gefluc Marseille-Provence.

* To whom correspondence should be addressed. Tel: 491835505. Fax: 491782024. E-mail: peyrot@pharmacie.univ-mrs.fr.

‡ UMR-CNRS 6032, Faculté de Pharmacie.

§ Laboratoire de Biophysique 1, Faculté de Pharmacie.

[1] Abbreviations: C52, cryptophycin 52; EDTA, ethylenediaminetetraacetic acid; EGTA, ethylene glycol bis(β-aminoethyl ether)-*N*,*N*,*N*′,*N*′-tetraacetic acid; GTP, guanosine triphosphate; GDP, guanosine diphosphate; HPLC, high-performance liquid chromatography; MAPs, microtubule-associated proteins; Me_2SO, dimethyl sulfoxide; PDB, Protein Data Bank (http://www.rcsb.org/pdb/); PG buffer, 20 mM sodium phosphate−0.1 mM GTP, pH 7.0; SDS, sodium dodecyl sulfate; RASMB, reversible associations in structural and molecular biology (http://www.bbri.org/rasmb/rasmb.htlm).

10.1021/bi010926z CCC: $20.00
Published on Web 10/17/2001

al. (*11*), studying the binding of radiolabeled C52 to tubulin, found that C52 binds tightly to a single high-affinity site in tubulin and that C52 binding changes the tubulin conformation. However, there is no observation indicating that C52 binding depends on tubulin concentration, suggesting that C52 does not induce tubulin self-association. Finally, competition experiments supported the fact that the C52 binding site may overlap with the vinblastine binding site (*6*, *8*, *11*).

To further understand the mechanism of action of cryptophycin 52 and the molecular basis of its action, we analyzed the interaction of C52 with microtubules and tubulin in vitro through turbidimetric measurements of microtubule assembly, analytical ultracentrifugation, and electron microscopy. In addition, combining the experimental results with the three-dimensional structure of tubulin and molecular modeling methods, we propose a structure of cryptophycin 52 within its binding site on the tubulin dimer and a kinetic pathway for its mechanism of action.

MATERIALS AND METHODS

Pig brains were obtained from freshly slaughtered animals, kept on ice, and used within 1 h after their death. Cryptophycin 52 (C52) was a gift from Eli Lilly and Co., through the courtesy of Dr. Dan Williams, and was used without further purification. All other chemicals were of reagent grade.

Preparation of Pig Brain Tubulin. Tubulin was purified from pig brain by ammonium sulfate fractionation and ion-exchange chromatography. The protein was stored in liquid nitrogen and prepared as described (*12*−*14*). Protein concentrations were determined spectrophotometrically with an extinction coefficient of $\epsilon_{275nm} = 1.07$ L·g^{-1}·cm^{-1} in 0.5% SDS in neutral aqueous buffer or with $\epsilon_{275nm} = 1.09$ L·g^{-1}·cm^{-1} in 6 M guanidine hydrochloride. Most experiments were done in PG buffer (20 mM sodium phosphate−0.1 mM GTP, pH 7).

Tubulin Polymerization. Microtubule assembly was performed in 20 mM sodium phosphate buffer, 1 mM EGTA, 10 mM $MgCl_2$, and 3.4 M glycerol, pH 6.7. The reaction was started by warming the samples to 37 °C in thermostated cuvettes (1 × 0.2 cm), and the mass of polymer formed was monitored by turbidimetry at 350 nm with Beckman DU70 and DU7400 spectrophotometers. Samples containing C52 compound and their controls had less than 2% residual Me_2SO.

Microtubule Inhibition Data Analysis. The data on the inhibition of microtubule assembly by C52 were analyzed with the following equation given by Perez-Ramirez et al. (*15*):

$$F = \frac{1}{1 + K_b K_i \mathrm{Cr}[\mathrm{A}]} - \frac{K_b \mathrm{Cr}[\mathrm{A}]}{(T_{tot} - \mathrm{Cr})(1 + K_b K_i \mathrm{Cr}[\mathrm{A}])}$$

F is the fraction of turbidity measured in the presence of an inhibitor relative to that in its absence. By an iterative procedure we calculated K_i, the strength of the inhibitory capacity of the drug, K_b, the affinity binding constant, and [A], the free ligand concentration. The free ligand ($[A] = [A]_{tot} - [A]_{bound}$) concentrations were calculated by solving the equation $[A]_{bound} = {}^1/_2\{([A]_{tot} + [T]_{tot} + K_d) - (([A]_{tot} + [T]_{tot} + K_d)^2 - 4[T]_{tot}[A]_{tot})^{1/2}\}$, where $[A]_{tot}$ is the total ligand concentration, $[T]_{tot}$ is the total protein concentration, and K_d is K_b^{-1}. We used a commercial graphics/curve fitting program (Sigmaplot 4.0, Jandel Scientific). The algorithm for this software starts with an arbitrary opening set of K_i and K_b values. With these values, [A] and $[A]_{bound}$ are calculated and then the nonlinear least-squares regression analyses are executed. The initial set is corrected in the next step by the Marquardt−Levenberg procedure. This iterative procedure is continued until one obtains the minimum sum of squared deviations between experimental and calculated values of F.

Preparation of GTP−Tubulin. Aliquots of protein were chromatographed in drained spin columns (1 × 6 cm) of Sephadex G25, equilibrated with PG buffer, and then passed through a larger (1 × 10 cm) gravity column of Sephadex G25 equilibrated with PG buffer. This standard preparation consists of about 93% GTP-liganded tubulin at the exchangeable site and contains residual Mg^{2+} (*16*).

Preparation of GDP−Tubulin. Tubulin with GDP occupying the exchangeable site (E-site) was prepared by the two-step exchange procedure described by Diaz and Andreu (*16*). Protein samples were passed through a drained centrifuge column of Sephadex G25 medium (1 × 6 cm) equilibrated with 20 mM sodium phosphate buffer, 1 mM EDTA, and 1 mM GDP, pH 7 in the cold. GDP (10 mM) was added to the protein, which was incubated on ice for 10 min. A second cold Sephadex G25 chromatography (1 × 10 cm) equilibrated with the same buffer served to remove the excess nucleotide. HPLC analysis of the resulting protein showed that it contained 99% GDP at site E (*17*).

Chemicals. Cryptophycin 52 stock solution was prepared in Me_2SO and kept at −20 °C. The extinction coefficient, ϵ, was determined by dissolving dry crystals of the compound in Me_2SO and then diluting the solution in ethanol. The UV−visible spectra were then recorded. Three independent determinations gave $\epsilon_{280nm} = 2132 \pm 43$ M^{-1}·cm^{-1}.

Measurements of the Stoichiometry of C52 in Rings by Cosedimentation Assay. Tubulin and tubulin plus an excess of C52 were centrifuged at 20 °C for 50 min at 100 000 rpm in a TLA 100.2 rotor in a TL100 ultracentrifuge (Beckman), using 1 mL polycarbonate tubes. At the end of the centrifugation, the upper half and the lower part of the tube (500 μL) were carefully withdrawn, and the protein concentration was determined spectrometrically in 6 M guanidine hydrochloride. The upper half contained almost no protein, and the lower half contained free proteins that had not formed rings. Tubulin concentration in the pellet (rings) was calculated by subtracting the protein concentration in the lower part of the supernatant with C52 from the protein concentration without C52. The pellet was resuspended in ethanol, tubulin was precipitated by 0.5 M perchloric acid and centrifuged at 20000*g* for 10 min at 4 °C, and the absorbance of the supernatant was measured at 280 nm. To determine the concentration of C52 in the ring, we subtracted from this supernatant absorbance the absorbance of the nucleotides extracted from the exchangeable and nonexchangeable site of tubulin, using an extinction coefficient of 8065 M^{-1}·cm^{-1} at 280 nm.

Electron Microscopy. Small aliquots of the solution were adsorbed to carbon-coated Formvar films on copper grids, stained for 1 min in 2% uranyl acetate, and observed with a JEOL 1200 electron microscope.

Sedimentation Velocity. The experiments were done at 40 000 rpm and 20 °C in a Beckman Optima XL-A analytical ultracentrifuge equipped with absorbance optics, using an An55Ti rotor and 3 mm double-sector centerpieces. The apparent sedimentation coefficients were determined by fitting the velocity data using three noninteractive species with the SEDFIT program (*18*) and corrected to the standard conditions by the SEDNTERP program (retrieved from the RASMB server). Apparent sedimentation coefficient distributions, $g(s)$, were generated by least-squares boundary modeling of sedimentation velocity data by the SEDFIT program and the DCDT program (*19*), also taken from the RASMB server. From both methods we obtained similar apparent sedimentation coefficient distributions.

Calculation of the Sedimentation Coefficient. All calculations were done using HYDRO; the hydrodynamics of the tubulin dimer were based on the X-ray scattering as described by Diaz et al. (*20*). HYDRO is a subroutine for the calculation of hydrodynamic properties of bead models of rigid macromolecules (*21*).

Molecular Modeling. Models were obtained with the Insight II, Biopolymer, Docking, and Discover software from MSI Technologies, Inc. (CA), running on a Silicon Graphics R10000 workstation. The pH was set to 6, and models were optimized with the CVFF force field. The cryptophycin 52 molecule was constructed and optimized with Biopolymer software. Complexes (C52−tubulin and tubulin−tubulin) were assembled with Docking to evaluate intermolecular energy and with Discover. A first step of energy minimization was carried out with a gradient conjugate algorithm down to a maximum derivative of 0.001 kcal/Å. Then, a dynamic step was performed at 300 K for 1.1 ps. The trajectory was analyzed with 110 complexes selected every 10 fs for the dynamic step. The low-energy complex was selected from this trajectory. Then, a second step of minimization with gradient conjugate algorithm was performed to refine complex models.

RESULTS

Microtubule Formation and C52. The inhibition of tubulin self-assembly into microtubules as a function of C52 concentrations is presented in Figure 1A. The rate of assembly as well as the final extent of assembly was reduced by C52. Figure 1B shows that the turbidity generated by the self-assembly of 22 μM pure tubulin was reduced by half at 2.75 μM C52, i.e., at a concentration 8 times lower than that of the tubulin concentration. Figure 1C shows that the extent of inhibition by C52 increased monotonically with the mole ratio of the total ligand to total protein in the solution. In this figure, 50% inhibition occurred at a mole ratio of 0.12 mol of C52/mol of tubulin, which indicated a substoichiometric mode of inhibition. Substoichiometric means the blocking of microtubule growth by the binding of either a tubulin−drug complex or a drug molecule to the growing polymer (*22*). For inhibition by colchicine, the blocking entity is the stable tubulin−colchicine complex. The simplest mechanism that can quantitatively describe the inhibition process is given by Perez-Ramirez et al. (*15*):

$$M_{n-1}TA \overset{K_i}{\longleftrightarrow} TA + M_{n-1} \overset{K_b}{\longleftrightarrow} A + T + M_{n-1} \overset{K_g}{\longleftrightarrow} M$$

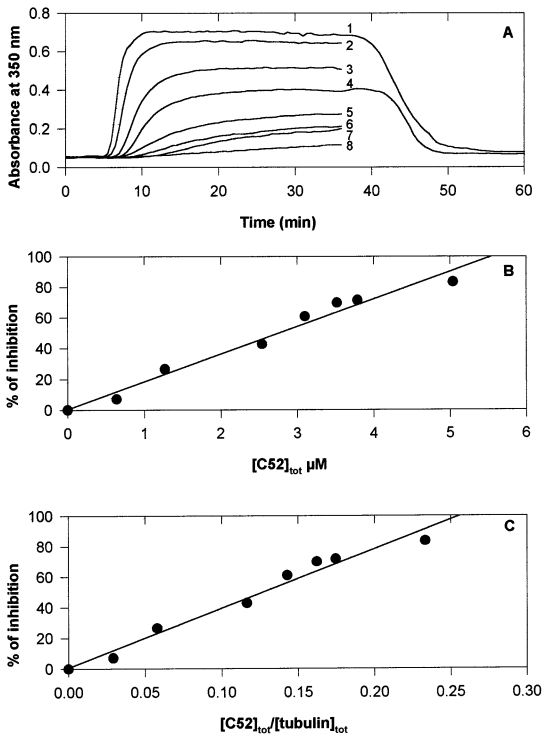

FIGURE 1: Effects of C52 on tubulin polymerization. (A) Concentration dependence curves for inhibition of polymerization by C52: (1) 22 μM tubulin; (2−8) same as (1) with 0.6, 1.3M, 2.5, 3.1, 3.5, 3.8, and 5.0 μM C52. At 35 min the samples were cooled to 10 °C; in all cases the turbidity decreased to the original values. (B) Fraction of the reduction of the plateau absorbance values (inhibition) as a function of the total C52 concentration. (C) Fraction of the reduction of the plateau absorbance values (inhibition) as a function of the ratio of the total C52 concentration to total tubulin concentration.

In this scheme K_g is the normal microtubule growth constant, equal to Cr^{-1} (Cr is the critical concentration without drug; see Figure 2A; Cr was 0.55 mg/mL); K_b is the binding constant of the drug to tubulin; K_i is the microtubule inhibition constant, which is the binding constant of the tubulin−drug complex to the end of a growing microtubule, the consequence of which is the stopping of microtubule assembly; A is the free drug; T is the free tubulin; M_{n-1} is the microtubule before elongation; and M is the microtubule after addition of one tubulin. This scheme leads to the equation (see ref *15* for details):

$$F = \frac{1}{1 + K_b K_i \mathrm{Cr}[\mathrm{A}]} - \frac{K_b \mathrm{Cr}[\mathrm{A}]}{(T_{tot} - \mathrm{Cr})(1 + K_b K_i \mathrm{Cr}[\mathrm{A}])} \quad (1)$$

where F is the fraction of turbidity measured in the presence of an inhibitor relative to that in its absence. Perez-Ramirez et al. (*15*, *23*) determined the value of K_i, taking the values of K_g and K_b from previous works. In fact, the above equation can be used to calculate by an iterative procedure the apparent constants K_i, the strength of the inhibitory capacity of the drug, K_b, the affinity binding constant, and [A], the free ligand concentration (see Materials and Methods).

First, we evaluated the reliability of the above iterative method. We used the inhibition data of TMB (2,3,4,4′-tetramethoxy-1,1′-biphenyl), an extensively characterized analogue of colchicine (the literature data were taken from ref *15*; Figure 1A). The inhibition data of TMB fit (Figure

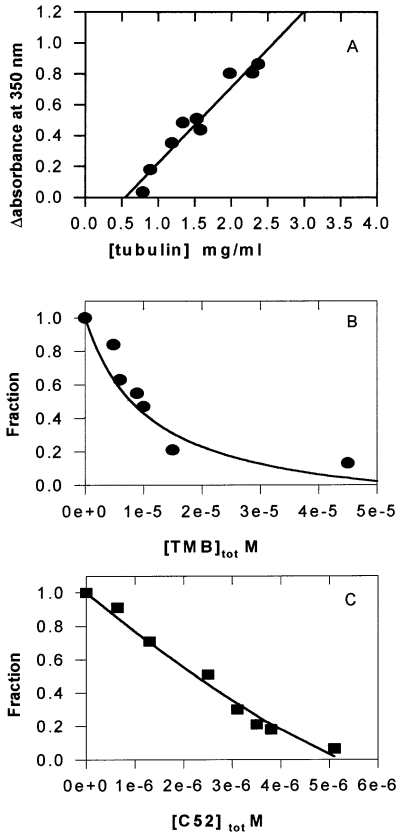

FIGURE 2: Inhibition data analysis. (A) Critical concentration plot representing the amount of polymerized tubulin versus the total concentration of tubulin. The abscissa intercept represents the concentration of unassembled tubulin at steady state (Cr). (B) Inhibition of tubulin self-assembly as a function of the total TMB concentration. The solid line is the theoretical curve obtained by simultaneous fitting of K_i, K_b, and drug concentrations to eq 1. (C) Inhibition of tubulin self-assembly (22 μM) as a function of the total C52 concentration. The solid line is the theoretical curve obtained by simultaneous fitting of K_i, K_b, and drug concentrations to eq 1.

2B) with $K_b = (3.1 \pm 2.1) \times 10^4$ M^{-1} and $K_i = (3 \pm 2) \times 10^5$ M^{-1}. The values of Medrano et al. (*24*) and Perez-Ramirez et al. (*15*) for K_b and K_i were 8.2×10^4 M^{-1} and $(9.60 \pm 1.34) \times 10^4$ M^{-1}, respectively. These values were similar to those calculated by our iterative procedure, suggesting that our analysis is accurate. The simplicity of the model and of the iterative procedure makes it easy to calculate the apparent affinity constant K_b and inhibition constant K_i from turbidity data.

Consequently, we used this method for C52. The inhibition results (Figure 2C) are presented in the form of fractions as a function of total C52 concentrations. We calculated $K_b = (3.0 \pm 1.1) \times 10^6$ M^{-1} and $K_i = (1.9 \pm 0.3) \times 10^5$ M^{-1}. Panda et al. (*11*) determined the binding of C52 to tubulin at 34 °C (a temperature similar to that used for microtubule formation, 37 °C) by analyzing the effects of C52 on the intrinsic tryptophan fluorescence of tubulin. They found an apparent affinity constant of 3.6×10^6 M^{-1}. This result agrees closely with ours. However, Panda al. (*10*) using [^{3}H]C52 found that C52 bound as a C52−tubulin complex to microtubule ends in vitro with a very high apparent affinity binding constant of 2×10^7 M^{-1}. By the above method, we calculated $K_i = 1.9 \times 10^5$ M^{-1}. This huge discrepancy between the two results indicated that analyzing the C52

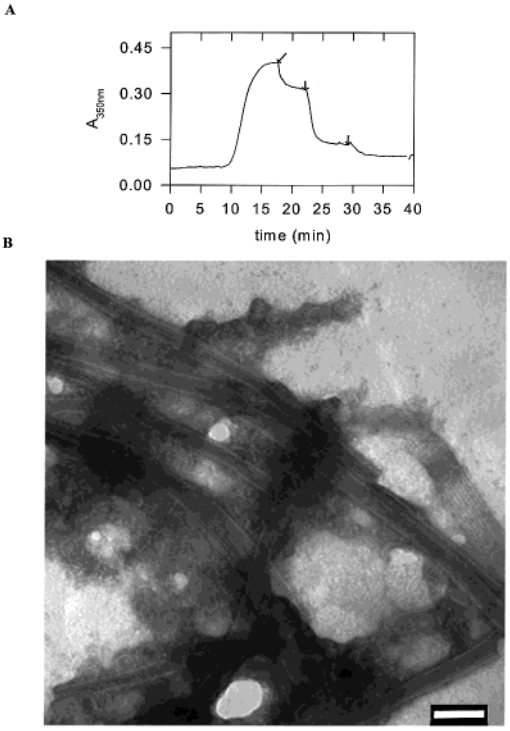

FIGURE 3: Effects of C52 on assembled microtubules. (A) Effects of various C52 concentrations on assembled microtubules. Each arrow corresponds to the addition of 4 μM C52. (B) Electron microscopy of C52-treated microtubules after addition of 4 μM C52 (after the first arrow). The bar represents 50 nm.

inhibition data in terms of equilibria as described in the scheme above does not reflect the mechanism of action of C52. Indeed, the equilibrium model adopted in this study relies on an important assumption, that is, the binding constant of the ligand must be independent of protein concentration, which might not be the case for C52. Furthermore, microtubule inhibition by C52 may involve the binding of more than one C52 molecule to a microtubule [for the limits of the model, see Perez-Ramirez's discussion (*15*)].

To establish whether the binding reaction depends on protein−protein interactions, we verified the association state of tubulin in the presence of C52 by sedimentation velocity measurements. In nonassembly conditions (tubulin is unable to form microtubules) C52 induced changes in the sedimentation pattern of tubulin. For example, 50% of the tubulin (5.8S) was self-assembled into 8−9S oligomeric species at a mole ratio of 0.12 mol of C52/mol of tubulin. This result demonstrates that C52 induces significant self-association of tubulin heterodimer. This suggested that the mechanism of binding of C52 is a ligand-induced self-association of tubulin in which the binding of the ligand to tubulin dimers precedes the macromolecular self-association. Therefore, the binding parameters determined by Panda et al. (*11*) and our calculated constant K_b reflected the macroscopic apparent equilibrium constant, which depended highly on the buffer conditions (presence or absence of Mg^{2+}; magnesium ions enhance the self-association of tubulin) and tubulin concentrations.

To gain further information on the mechanism of action of C52, we checked this drug on assembled microtubules (Figure 3A). A sample of 15 μM tubulin was polymerized

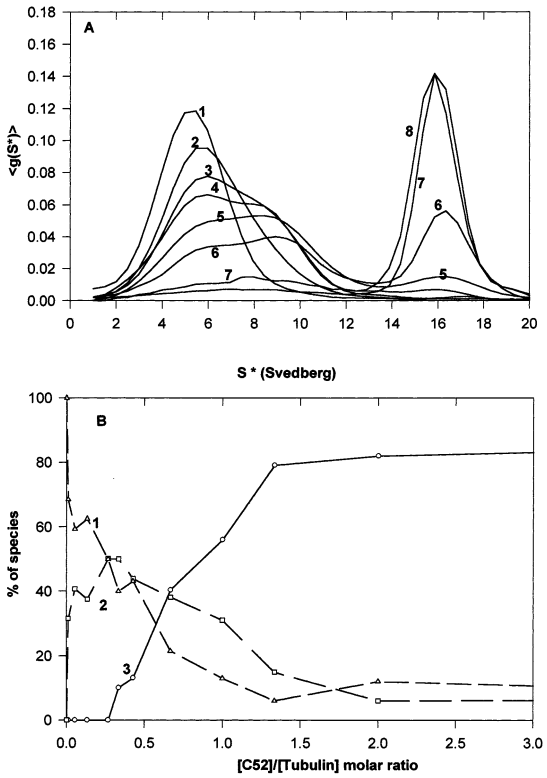

FIGURE 4: Effects of C52 on tubulin self-association. (A) Distribution of the sedimentation coefficients of tubulin (15 μM) in the absence of C52 (1) and in the presence of 0.8 μM (2), 4 μM (3), 5 μM (4), 6.4 μM (5), 10 μM (6), 20 μM (7), and 125 μM (8) C52. (B) Sedimentation velocity patterns of tubulin (15 μM) in the presence of C52 analyzed in terms of three components, a heavy 15−17S component (circles), an 8−9S species (squares), and a 5.7S species (triangles). The percent of tubulin in each species was plotted versus the C52:tubulin molar ratio.

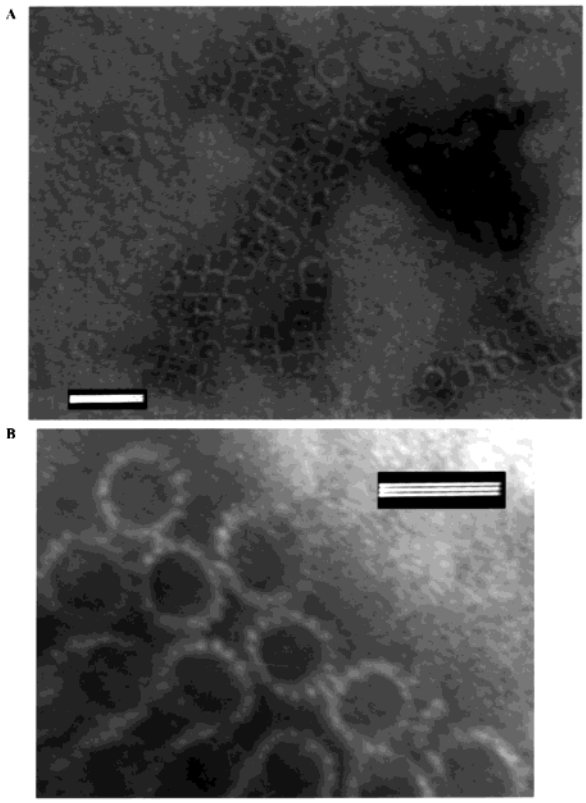

FIGURE 5: Electron micrographs of C52-induced tubulin aggregates. (A) The morphology of tubulin aggregates induced by 50 μM C52. The bar represents 80 nm. (B) Single ring structures at high magnification. The bar represents 50 nm.

to plateau turbidity, after which addition of 4 μM C52 induced a decrease in turbidity. Electron microscopic examination revealed the presence of microtubules, rings, opened microtubules, and sheets (Figure 3B). Adding another 4 μM C52 induced a large decrease in turbidity; electron microscopy showed some microtubules and many single rings. Finally, addition of another 4 μM C52 induced complete depolymerization; electron microscopy showed only rings. A slight residual turbidity suggested that microtubules were dissociated into small nonscattering rings. With paclitaxel-stabilized microtubules, we obtained similar results with a slower depolymerization rate (data not shown).

Ring Formation and C52. In the above experiments we observed that the binding of C52 to tubulin induced the self-association of tubulin. The self-association of 15 μM GTP−tubulin in the presence of C52 from 0.16 to 125 μM was then studied in a magnesium-free buffer by sedimentation velocity at 20 °C. Figure 4A shows sedimentation coefficient distributions, $g(s)$, calculated from the sedimenting boundary. In phosphate buffer, tubulin sedimented as a single species of 5.7S (profile 1). With an excess of C52 (50 and 125 μM), tubulin sedimented as a single species at 16−17S with a slight spreading shoulder at about 8−9S (profiles 7 and 8). At intermediate concentrations of C52, tubulin sedimented as three interacting components (see profiles 5 and 6), indicating that these species were in a rapid equilibrium. Apparent sedimentation coefficient values were calculated and expressed in percentage as a function of a molar ratio between the C52 and tubulin concentrations (Figure 4B). The proportion of tubulin 5−6S species (curve 1) decreased and reached a minimum (10%) for a ratio of 1. The intermediate species (8−9S) (curve 2) reached a maximum of 50% for a ratio of C52 to tubulin of about 0.3, and then this percentage decreased (to 10%); simultaneously, the 16−17S species increased (curve 3) to 80% for a molar ratio of 1.3 mol of C52/mol of tubulin. No other species was observed upon increasing the C52 concentration to 125 μM (data not shown), i.e., to an 8.3 molar ratio of C52 to tubulin. These results demonstrate that C52 induces tubulin oligomerization into complexes sedimenting at 8−9S and at 16−17S. Beyond a molar ratio of 2, the 16−17S tubulin−C52 complex is the main species. In other terms the apparent sedimentation coefficient reached a plateau. This behavior is consistent with a self-associating system that proceeds to an end-state polymer via a chain growth process, the free energy of formation of the final polymer being highly favorable (*25*). However, we cannot rule out another model in which a self-association process terminates at a given stoichiometry without any favorable free energy change for the formation of the end product (*26*). To gain insight into the nature of the self-association, we examined by electron microscopy samples of GTP−tubulin complexed by C52 in phosphate buffer (pH 7) with 0.1 mM GTP at 20 °C (Figure 5). The micrographs revealed the presence of ring-like structures and a background of ring fragments. These thin rings were the only protein aggregates seen with a distinct geometrical configuration; no filamentous or rod-shape structures were seen under these conditions (Figure 5A). Several distorted views of the structure were apparent, suggesting ring opening,

folding, or partial raveling. The overall appearance was that structures were single rings composed of a single layer of tubulin subunits (Figure 5B). The outside diameter of the single rings was 28 ± 3 nm. The inner diameter was 19 ± 2 nm. Considering that a tubulin dimer is 8 nm long (*27*), this corresponds to 9.4 ± 0.8 dimer rings.

To further characterize these ring structures, we measured the sedimentation coefficient of these single rings by analytical velocity experiments. Extrapolation of data collected at different tubulin concentrations (between 1.5 and 0.5 mg/mL) to zero protein concentration yields a sedimentation coefficient $s^0_{20,w}$ of 17.9 ± 0.3 S. Then, the theoretical sedimentation coefficient of a nine-dimer ring was calculated by HYDRO. We obtained a sedimentation coefficient of 18.1 S, which is in good agreement with our experimental value.

By cosedimentation assay (see Materials and Methods), a stoichiometry of 1.3 ± 0.2 was obtained, confirming the result by ultracentrifugation. All together, these results demonstrate that C52 induces the self-association of tubulin into nine-dimer single ring oligomers (end product) and that it is able to form rings from both polymerized (microtubule) and nonpolymerized tubulin.

At high millimolar concentrations (16 mM) of Mg^{2+} ions, GTP−tubulin can spontaneously assemble into double ring-shaped oligomers. The effects of C52 on the formation of double rings were examined in the analytical ultracentrifuge (Figure 6A). Without C52, tubulin (50 μM) sedimenting at about 7.4S was in equilibrium with a population of oligomers sedimenting as one species at 35S (full line). Upon addition of 50 μM C52 (dotted line) we observed only one species sedimenting at 15−16S. This showed that C52 inhibits the oligomerization of tubulin into double rings and that it has a high tendency to associate tubulin into single rings. This result was confirmed by examination of samples by electron microscopy (Figure 6B). Here, the single rings formed in the presence of 16 mM Mg^{2+} were visually denser and stronger than those obtained without Mg^{2+}. GDP−tubulin dimers had a much stronger propensity to form double rings than did GTP−tubulin. Sedimentation patterns of GDP−tubulin (10 μM) with C52 (85 μM) showed that GDP−tubulin sedimented as one species at 16−17S, indicating that C52 inhibited the tubulin association leading to double ring formation (data not shown). Electron microscopy revealed single rings (data not shown).

Modeling of Cryptophycin 52 in Its Putative Binding Site. Cryptophycin 52 (Chart 1) is a small molecule containing two aromatic rings able to form hydrophobic interactions with tubulin. The C52 chemical structure was built and optimized by molecular modeling (Figure 7). The two phenyl rings on each side of the C52 compound can rotate around the carbon−carbon bond. Moreover, C52 has three carbonyl oxygen groups able to create hydrogen bonds with NH and/or SH groups of tubulin amino acids.

Several experiments have shown that cryptophycin binds to tubulin in the vicinity of or in the vinca alkaloid binding site (*6*, *8*, *11*). This vinblastine binding site has been identified by tryptic hydrolysis on β-tubulin, between residues 175 and 215. The electron crystallographic model structure of the $\alpha\beta$-tubulin dimer was established in 1998 by Nogales et al. (*27*). Coordinates are available in Protein Data Bank (PDB, code 1TUB) and served us as a model to

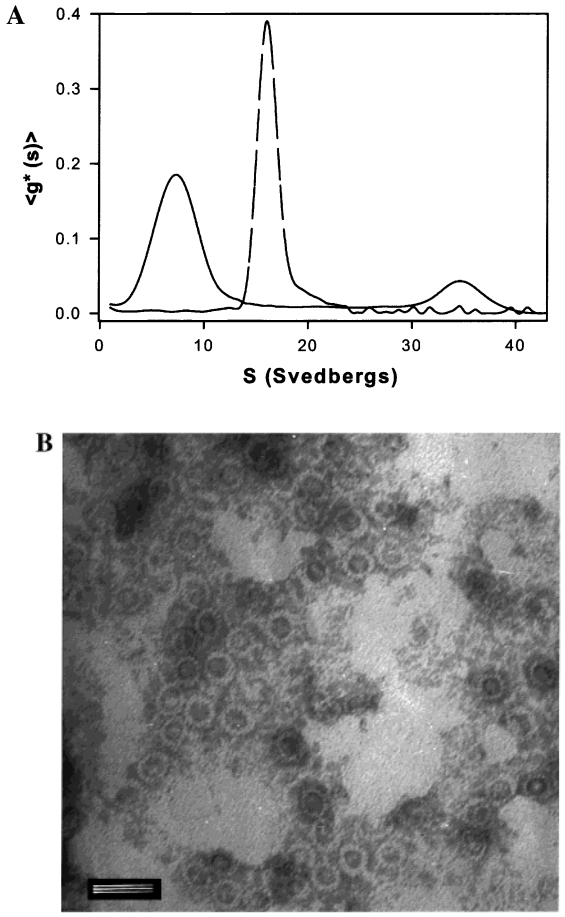

FIGURE 6: C52 induces dissociation of double ring oligomers to single ring oligomers. (A) Distributions of the sedimentation coefficients of GTP−tubulin (50 μM in 20 mM phosphate buffer, pH 6.5, containing 0.1 mM GTP and 16 mM Mg^{2+}) in the absence (solid line) and in the presence of 50 μM C52 (dashed line). (B) Electron micrograph of GTP−tubulin in the presence of 16 mM Mg^{2+} and 100 μM C52, showing single rings. The bar represents 50 nm.

reconstruct a three-protofilament portion of a microtubule (Figure 8). A microtubule is a bidimensional lattice in which tubulin subunits interact via longitudinal bonds (along protofilaments) and lateral bonds (between adjacent protofilaments) (*28*). Longitudinal bonds are implicated in both $\alpha-\beta$ intradimer and $\beta-\alpha$ interdimer interactions. These bonds involve interactions between the helix H6, the loop H6−H7, and the helix H10. Lateral bonds concern $\alpha-\alpha$ and $\beta-\beta$ interactions also involving H6 helix and H6−H7 loop. In our reconstructed model, the vinblastine binding site is not accessible to solvent except for two regions on the outside of the microtubule: residues 188−197 and 205−215 (helix H6) (Figure 8). The 188−197 region does not seem to be involved in contacts between tubulin dimers along the microtubule (*28*, *29*). The 205−215 domain is at the interface between two protofilaments and is involved in several lateral contacts (*28*, *29*). Thus, this surface is a good candidate for the binding site of ligands that disrupt the microtubule. Moreover, in the vinblastine binding site, there are two cysteines (Cys 201 and Cys 211) that could form a hydrogen bond with drugs (*30*); Cys 201, however, is buried in a β-sheet inside the monomer of β-tubulin, making it inaccessible. In contrast, Cys 211 has a great solvent accessibility and could bind to exogenous ligands. Moreover, there are

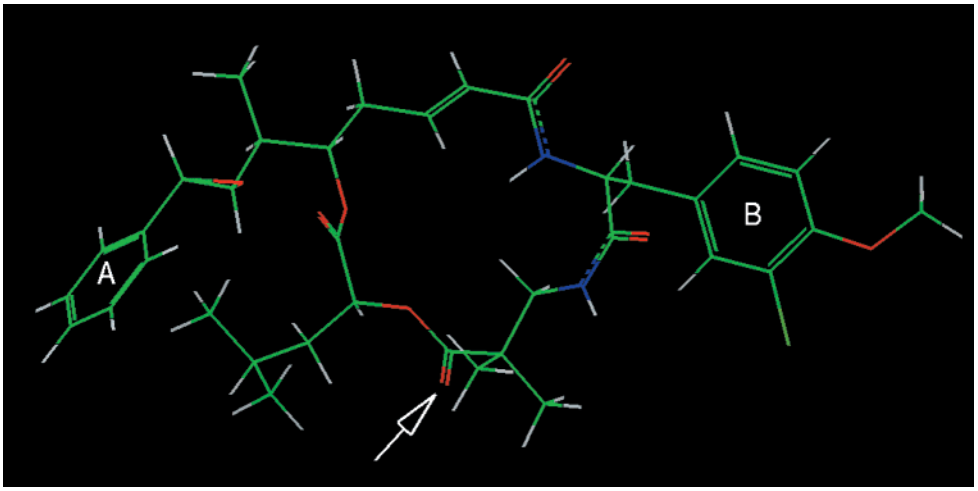

FIGURE 7: Molecular minimized structure of cryptophycin 52. Carbon is in green, oxygen in red, nitrogen in blue, and chloride in yellow. C52 contains two aromatic rings, A and B. The arrow indicates the carbonyl oxygen that could form a hydrogen bond with NH and/or SH groups of tubulin amino acids.

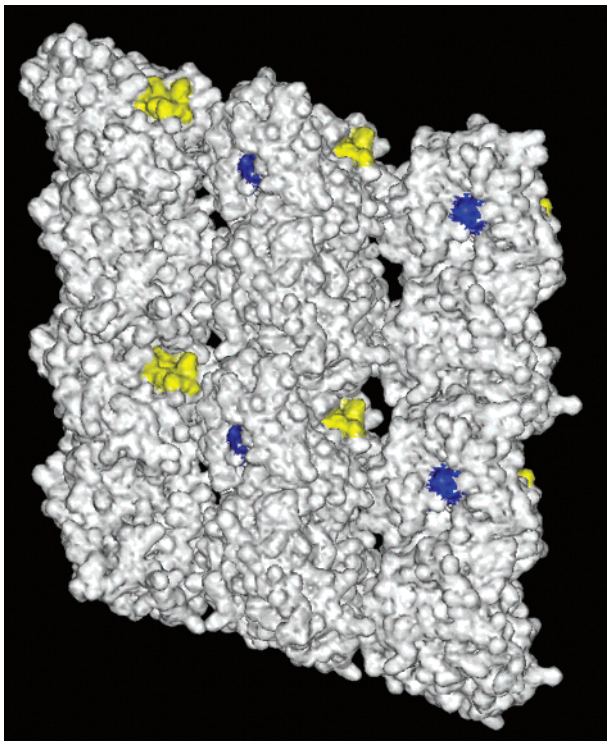

FIGURE 8: Reconstruction of three adjacent protofilaments. This model shows a front view of the solvent-accessible surface of the potential C52 binding site on β-tubulin at the outside surface of a microtubule. Two regions are notably accessible to solvent on β-tubulin: residues 188−197 in blue and residues 205−215 in yellow. The latter is at the interface between two protofilaments.

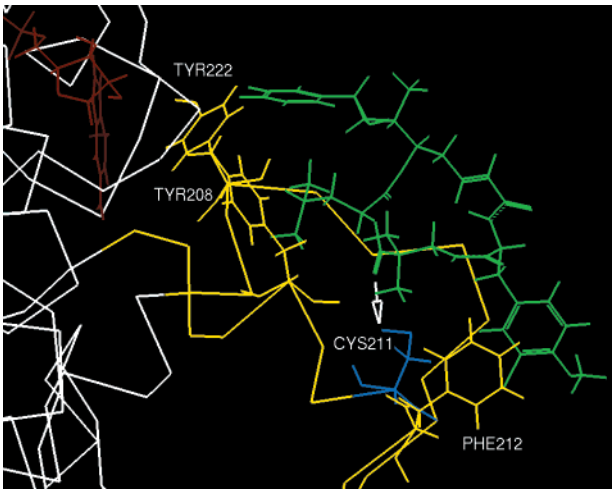

FIGURE 9: Molecular modeling of the cryptophycin 52 binding in the electron crystallographic structure of β-tubulin. C52 is in green. The backbone of the cryptophycin binding site, in yellow, is between residues 204 and 225. For C52 we chose the best molecular orientation fitting in this pocket. One hydrogen bond (white arrow) can be formed between a carbonyl oxygen group of C52 and the SH group of Cys 211 (in blue). Each phenyl ring of C52 interacts with aromatic rings in the vicinity. In this model, the phenyl ring A interacts with Tyr 208 and Tyr 222, and the phenyl ring B interacts with Phe 212. The cryptophycin binding site is near the exchangeable GTP binding site (GDP is in red).

several aromatic residues near Cys 211, which form a hydrophobic cluster able to interact with drugs such as cryptophycin and vinblastine.

Cryptophycin 52 was positioned in its potential binding site, i.e., pocket 205−215 near the Cys 211 on β-tubulin, and the molecular modeling of the complex was performed. In a radius of 10 Å, this pocket contained the helix H6 (residues 204−213), the H6−H7 loop (residues 214−221), and the beginning of helix H7. One hydrogen bond can be formed between a carbonyl group of C52 and the SH of the Cys 211 (Figure 9). Moreover, in our model some hydrophobic contacts between each phenyl of cryptophycin 52 and aromatic rings of Tyr 208, Phe 212, and Tyr 222 can be established (Figure 9).

Modeling of C52 Induced Rings. We found that C52 binds to tubulin and induces a conformational change leading to the formation of single rings. To further investigate this result, we modeled ring formation by computational analysis, using recent structural findings on stathmin−tubulin interaction. Stathmin is a phosphoprotein that interacts with the $\alpha\beta$-tubulin heterodimer and modifies microtubule dynamics (*31*). The crystal structure of the GDP−tubulin−stathmin-like domain complex has been determined (*32*). Coordinates of two tubulin heterodimers complexed by the stathmin-like domain are available in the PDB (1FFX). The binding of stathmin to the tubulin dimer induces a curvature very similar to the one of depolymerization products of microtubules induced by cold (*33*) and of GDP−tubulin oligomers (rings).

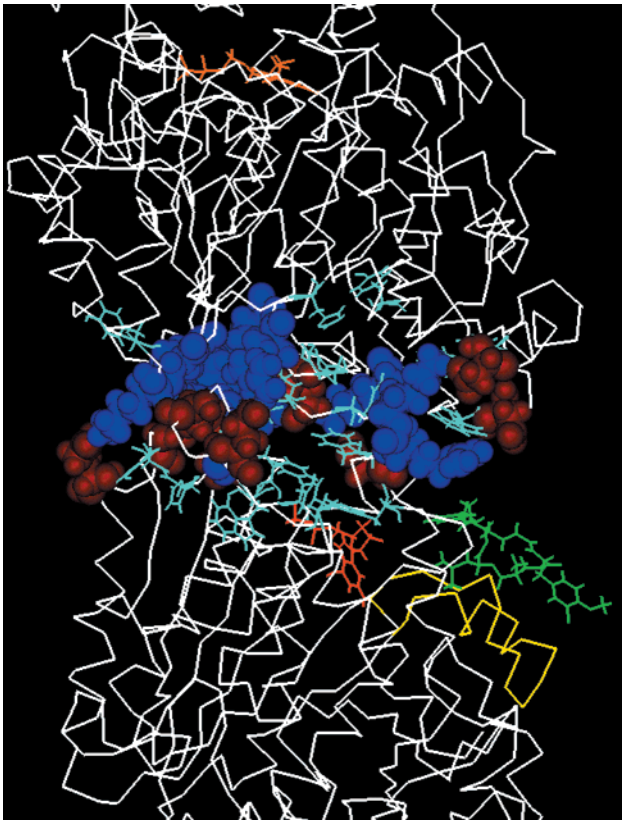

FIGURE 10: Molecular modeling of the electrostatic and hydrophobic $\beta-\alpha$ interdimer contacts. Cryptophycin 52 is in green and its binding site is in yellow. GDP bound to β-tubulin and GTP bound to α-tubulin are in red and orange, respectively. The backbone of $\beta-\alpha$ interdimer is in white. Lateral chains of aromatic residues are shown in light blue. Basic residues in deep blue (CPK mode) were located mainly on the α-tubulin side whereas acidic residues in red (CPK mode) were on the β-tubulin side. The curvature brings these charged residues as well as the hydrophobic amino acids closer to each other, stabilizing the interdimer contacts.

The repetition of the stathmin−tubulin unit results in the formation of a spiral structure formed by 16 tubulin dimers with a diameter of 40 nm (*32*). Stathmin modifies both the $\alpha-\beta$ intradimer and the $\beta-\alpha$ interdimer contacts. Interestingly, these modifications involve the hypothetical C52 binding site.

We demonstrated above that C52 binding provokes the formation of nine-dimer single rings with a stoichiometry of one molecule of C52 per tubulin dimer. The outside diameter of rings visualized by electron microscopy was about 30 nm, which is smaller than stathmin−tubulin spiral structures. From the stathmin−tubulin complex and from the $\alpha\beta$ dimer structure in a microtubule determined by Nogales et al. (*28*), we did molecular reconstruction of a ring with C52-liganded tubulin. We built a tetrameric model with $\alpha-\beta$ intradimer contacts maintained as in the microtubule and with $\beta-\alpha$ interdimer contacts with a curvature similar to the one found in the stathmin−tubulin dimer.

To construct such a single ring, the interdimer contacts between two $\alpha\beta$ dimers must produce a bigger curvature than with stathmin. To obtain the final tetrameric unit for the C52 ring, a slight rotation between the two $\alpha\beta$ dimers had to be done. The interdimer contacts were modeled and minimized, giving the final orientation of two successive dimers in a ring. Basic residues were located essentially on the α-tubulin side whereas acidic residues were on the β-tubulin side (Figure 10, Table 1A). After energy minimization and dynamic simulation, the lateral chains of the charged amino acids formed several electrostatic bonds at a distance smaller than 3 Å. Several aromatic and other hydrophobic amino acids were present in this region and were probably involved in hydrophobic $\beta-\alpha$ interdimer contacts stabilizing the ring (Table 1B). At last, to reconstruct the complete ring, each tetramer unit was half-superimposed over the previous one. We obtained a single ring formed by nine $\alpha\beta$-tubulin dimers (Figure 11). In the modeling process, however, a

Table 1: Putative Interdimer Contacts in a Ring

α	β
(A) Electrostatic Bonds between α- and β-Monomers Connected by Molecular Modeling[a]	
Arg +2	Glu −108
Lys +163	Glu −111
Lys +164	Glu −401
Arg +243	Glu −69
Glu −254	**Lys +103**
Arg +264	Glu −405
Asp −345	**Arg +391**
Lys +352	Asp −177
Asp −438	**Lys +392**
(B) Aromatic Residues in the Interdimer Region[b]	
Tyr 161	Trp 101
Phe 255	His 105
Tyr 262	Tyr 106
His 266	Tyr 183
Phe 343	Phe 385
Trp 346	Phe 389
Phe 351	His 396
Tyr 432	Trp 397
	Tyr 398
	Phe 394
	Phe 408

[a] The interdimer contact is polarized; most basic residues (in bold) are on α-tubulin and most acidic residues on β-tubulin. [b] A hydrophobic region is formed by a cluster of aromatic residues on both sides of the interacting tubulin subunit.

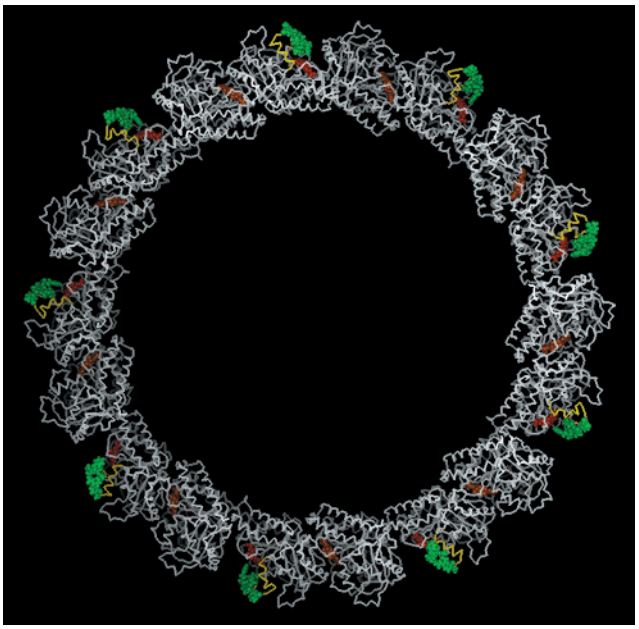

FIGURE 11: Ring reconstruction. The color code is identical to that in Figure 10. Nine molecules of C52 are bound to nine $\alpha\beta$ dimers of tubulin to form the final ring. Cryptophycin 52, GDP bound to β-tubulin, and GTP bound to α-tubulin are in CPK mode.

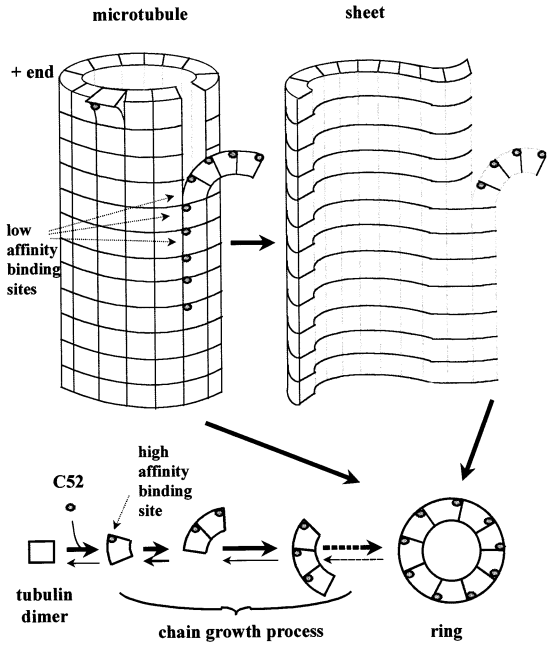

FIGURE 12: Kinetic scheme showing the mechanism of action of cryptophycin 52. On the upper part of the drawing is a microtubule with multiple C52 molecules bound along the microtubule surface. Such binding induces curvature, leading to the peeling away of the protofilaments. As the protofilament peels away, additional molecules of C52 bind to protofilament, which ultimately forms a ring. It is also shown that C52 binding is responsible for the opening of microtubules into sheets, also leading to ring formation. On the lower part of the picture is the C52 binding to soluble tubulin and inducing curvature in the tubulin dimer, leading to a chain growth process polymerization and finally the formation of a ring structure.

slight modification in the $\alpha-\beta$ interdimer angle led to the formation of rings ranging from eight to ten $\alpha-\beta$ dimers. Nevertheless, for the three types of rings the interactions described in Table 1 remained unchanged.

DISCUSSION

In a microtubule, the H6, H6−H7 region is at the interface between two protofilaments (*28*) and forms a pocket highly accessible to small hydrophobic drugs such as C52 or vinblastine. This region contains several electrostatic residues on α-tubulin that form a homogeneous hydrophilic surface and contains less hydrophilic residues on β-tubulin that form a hydrophobic surface accessible for C52, surrounded by few hydrophilic residues. This can also explain why vinblastine as well as C52 preferentially binds on β-tubulin. Docking of C52 into its hypothetical binding site on the helix H6, H6−H7 loop could induce the loss of longitudinal contacts between H6, H6−H7 regions of β-tubulin and the H10 of α-tubulin and the change in the interdimer contacts, leading to the destabilization of the microtubule and to the ring formation. In our model, the C52 binding site is located at the outside of a ring (Figure 11), which could explain why C52 inhibits by steric hindrance the formation of double ring.

A kinetic scheme showing the C52 induced pathway from tubulin or the microtubule to the ring is illustrated in Figure 12. Binding of a few C52 molecules per microtubule strongly suppresses the microtubule dynamic instability (*10*). This effect at very low concentrations suggests an action at microtubule ends (Figure 12). When 4−8 μM C52 was added to steady-state microtubules, we observed a depolymerization and the formation of rings and sheets. The formation of rings could easily be explained by binding of C52 to free tubulin (the Cr is about 0.6 mg/mL). The conformational change induced on tubulin by the binding of C52 provoked the self-association of tubulin dimers until a terminal step responsible for the closure of the ring polymer (Figure 12). The formation of tubulin sheets suggests that C52 might bind to the microtubule walls and open them by weakening the lateral interactions between the protofilament along the structural seam of the microtubule lattice. In that case, rings could also be directly formed by the closure of curved protofilaments, the core of a microtubule being in GDP−tubulin and thus with an intrinsic curved conformation.

Similar results were observed for microtubules stabilized by paclitaxel. However, in this case, the free tubulin concentration was very low (Cr near zero), which rules out an action on nonpolymerized tubulin only. How then can C52 form sheets and rings? It has been hypothesized (*34*) that taxoid-bound microtubules have great internal dynamics enabling the addition and the loss of protofilaments by a constant opening and closing of seams along the microtubule wall, even when their end-dynamic instability is frozen. We suggest that C52 binding favors the dissociation (opening) of the relatively weak lateral interactions between protofilaments, leading to the formation of opened microtubules and to the closure of curved protofilaments into rings.

Numerous studies report that cryptophycin 1 resembles vinblastine in its mode of action (*35*−*39*). Let us compare the mechanism of action of C52 and vinblastine. Cryptophycin 52, like vinblastine, has multiple effects on the properties of tubulin depending on their concentrations. At namomolar concentrations vinblastine, like C52, reduces the dynamic instability of microtubules (*35*). At micromolar concentrations vinblastine, like C52, blocks assembly of microtubules from tubulin dimers (*40*). For 10−200 μM concentrations (*41*), addition of vinblastine to microtubules at steady state causes their depolymerization and the formation of protofilament spirals and aggregates. This depolymerization occurs by stoichiometric binding of vinblastine to tubulin along the microtubule surface. Singer et al. (*41*), however, did not observe the formation of sheets or opened microtubules with vinblastine, yet we show that C52 was able to open microtubules. This discrepancy could be due to a difference in the affinity of both drugs for the microtubule surface. Furthermore, vinblastine at equimolar concentration also induces the formation of various tubulin polymers. This self-association of tubulin by vinblastine is consistent with an isodesmic indefinite type of self-association (*26*), characterized by weight-average sedimentation coefficients that do not reach a plateau, showing that there is no end product species. On the opposite hand, with C52 we demonstrated that the self-association proceeds to an end-state product (single rings) via an intermediate chain growth process. This particular behavior permits the two drugs to be distinguished.

In conclusion, C52 binds to the microtubule surface; such binding leads to peeling away of the protofilaments that ultimately form rings. We also show that C52 binds to soluble tubulin and induces a conformational change. This conformational change provokes the sequential oligomerization of tubulin, which also leads to the formation of a ring structure. Moreover, the binding of cryptophycin 52 to

tubulin depends on the tubulin concentration and induces changes in its sedimentation pattern. Now, to fully understand the mechanism of action of C52, it is necessary to analyze the association thermodynamics and the energy linkages between C52 binding and the self-association reactions.

ACKNOWLEDGMENT

We thank Dr. Leslie Wilson (UCSB, California) for helpful comments. We also thank S. Douillard (UMR-CNRS 6032) for assistance with protein purification and Dr. J. F. Diaz (CIB, SCIC, Madrid) for calculation of the sedimentation coefficients.

REFERENCES

1. Howard, W. D., and Timasheff, S. N. (1988) *J. Biol. Chem. 263*, 1342−1346.
2. Na, G. C., and Timasheff, S. N. (1982) *J. Biol. Chem. 257*, 10387−10391.
3. Schochet, S. S., Lampert, P. W., and Earle, K. M. (1968) *J. Neuropathol. Exp. Neurol. 27*, 645−658.
4. Lee, K. H. (1999) *J. Biomed. Sci. 6*, 236−250.
5. Schwartz, R. E., Hirsch, C. F., Sesubm, D. F., Flor, J. E., Chartrain, M., Fromtling, R. E., Harris, G. H., Salvatore, M. J., Liwaxh, J. M., and Yudin, K. (1990) *J. Ind. Microbiol. 5*, 113−124.
6. Bai, R., Schwartz, R. E., Kepler, J. A., Pettit, G. R., and Hamel, E. (1996) *Cancer Res. 56*, 4398−4406.
7. Panda, D., Himes, R. H., Moore, R. E., Wilson, L., and Jordan, M. A. (1997) *Biochemistry 36*, 12978−12953.
8. Smith, C. D., and Zhang, X. (1996) *J. Biol. Chem. 271*, 6192−6198.
9. Barrow, R. A., Hemscheidt, T., Liang, J., Paik, S., and Moore, R. E. (1995) *J. Am. Chem. Soc. 117*, 2479−2490.
10. Panda, D., Deluca, K., Williams, D., Jordan, M. A., and Wilson, L. (1998) *Proc. Natl. Acad. Sci. U.S.A. 95*, 9313−9318.
11. Panda, D., Ananthnarayan, V., Larson, G., Shih, C., Jordan, M. A., and Wilson, L. (2000) *Biochemistry 39*, 14121−14127.
12. Weisenberg, R. C., Borisy, G. G., and Taylor, E. W. (1968) *Biochemistry 7*, 4466−4479.
13. Lee, J. C., Frigon, R. F., and Timasheff, S. N. (1973) *J. Biol. Chem. 248*, 7253−7262.
14. Andreu, J. M., Gorbunoff, M. J., Lee, J. C., and Timasheff, S. N. (1984) *Biochemistry 23*, 1742−1752.
15. Perez-Ramirez, B., Andreu, J. M., Gorbunoff, M. J., and Timasheff, S. N. (1996) *Biochemistry 35*, 3277−3285.
16. Diaz, J. F., and Andreu, J. M. (1993) *Biochemistry 32*, 2747−2755.
17. Barbier, P., Peyrot, V., Leynadier, D., and Andreu, J. M. (1998) *Biochemistry 37*, 758−768.
18. Schuck, P., and Rossmanith, P. (2000) *Biopolymers 54*, 328−341.
19. Stafford, W. F. (1994) *Methods Enzymol. 240*, 478−501.
20. Diaz, J. F., Pantos, E., Bordas, J., and Andreu, J. M. (1994) *J. Mol. Biol. 238*, 214−225.
21. Garcia de la Torre, J., Navarro, S., Lopez Martinez, M. C., Diaz, F. G., and Lopez Cascales, J. J. (1994) *Biophys. J. 67*, 530−531.
22. Skoufias, D. A., and Wilson, L. (1992) *Biochemistry 31*, 738−746.
23. Perez-Ramirez, B., Gorbunoff, M. J., and Timasheff, S. N. (1998) *Biochemistry 37*, 1646−1661.
24. Medrano, F. J., Andreu, J. M., Gorbunoff, M. J., and Timasheff, S. N. (1991) *Biochemistry 30*, 3770−3777.
25. Frigon, R. P., and Timasheff, S. N. (1975) *Biochemistry 14*, 4559−4573.
26. Na, G. C., and Timasheff, S. N. (1980) *Biochemistry 19*, 1347−1354.
27. Nogales, E., Wolf, S. G., and Downing, K. H. (1998) *Nature 391*, 199−203.
28. Nogales, E., Whittaker, M., Milligan, R. A., and Downing, K. H. (1999) *Cell 96*, 79−88.
29. Meurer-Grob, P., Kasparian, J., and Wade, R. H. (2001) *Biochemistry 40*, 8000−8008.
30. Rai, S. S., and Wolff, J. (1996) *J. Biol. Chem. 271*, 14707−14713.
31. Belmont, L. D., and Mitchison, T. L. (1996) *Cell 84*, 623−631.
32. Gigant, B., Curmi, P. A., Martin-Barbey, C., Charbaut, E., Lachkar, S., Lebeau, L., Slavoshian, S., Sobel, A., and Knossow, M. (2000) *Cell 102*, 809−816.
33. Timasheff, S. N. (1991) *AIP Conf. Proc. 226*, 170−180.
34. Diaz, J. F., Valpuesta, J. M., Chacon, P., Diakun, G., and Andreu, J. M. (1998) *J. Biol. Chem. 273*, 33803−33810.
35. Toso, R. J., Jordan, M. A., Farrell, K. W., Matsumoto, B., and Wilson, L. (1993) *Biochemistry 32*, 1285−1293.
36. Jordan, M. A., Toso, R. J., Thrower, D., and Wilson, L. (1993) *Proc. Natl. Acad. Sci. U.S.A. 90*, 9552−9556.
37. Derry, W. B., Wilson, L., and Jordan, M. A. (1995) *Biochemistry 34*, 2203−2211.
38. Panda, D., Daijo, J. E., Jordan, M. A., and Wilson, L. (1995) *Biochemistry 34*, 9921−9929.
39. Panda, D., Jordan, M. A., Chin, K., and Wilson, L. (1996) *J. Biol. Chem. 271*, 29807−29812.
40. Owellen, R. J., Hartke, C. A., Dickerson, R. M., and Hains, F. O. (1976) *Cancer Res. 36*, 1499−1802.
41. Singer, W. D., Jordan, M. A., Wilson, L., and Himes, R. H. (1989) *Mol. Pharmacol. 36*, 366−370.

BI010926Z